Thermodynamic and Kinetic Characterization of Antisense Oligodeoxynucleotide Binding to a Structured mRNA

S. Patrick Walton,*† Gregory N. Stephanopoulos,† Martin L. Yarmush,* and Charles M. Roth*‡

*Center for Engineering in Medicine/Surgical Services, Massachusetts General Hospital, Harvard Medical School and Shriners Burns Hospital, Boston, Massachusetts 02114; †Department of Chemical Engineering, Massachusetts Institute of Technology, Cambridge, Massachusetts 02139; and ‡Departments of Chemical and Biochemical Engineering and Biomedical Engineering, Rutgers University, Piscataway, New Jersey 08854 USA

ABSTRACT Antisense oligonucleotides act as exogenous inhibitors of gene expression by binding to a complementary sequence on the target mRNA, preventing translation into protein. Antisense technology is being applied successfully as a research tool and as a molecular therapeutic. However, a quantitative understanding of binding energetics between short oligonucleotides and longer mRNA targets is lacking, and selecting a high-affinity antisense oligonucleotide sequence from the many possibilities complementary to a particular RNA is a critical step in designing an effective antisense inhibitor. Here, we report measurements of the thermodynamics and kinetics of hybridization for a number of oligodeoxynucleotides (ODNs) complementary to the rabbit β-globin (RBG) mRNA using a binding assay that facilitates rapid separation of bound from free species in solution. A wide range of equilibrium dissociation constants were observed, and association rate constants within the measurable range correlated strongly with binding affinity. In addition, a significant correlation was observed of measured binding affinities with binding affinity values predicted using a thermodynamic model involving DNA and RNA unfolding, ODN hybridization, and RNA restructuring to a final free energy minimum. In contrast to the behavior observed for hybridization of short strands, the association rate constant increased with temperature, suggesting that the kinetics of association are related to disrupting the native structure of the target RNA. The rate of cleavage of the RBG mRNA in the presence of ribonuclease H and ODNs of varying association kinetics displayed apparent first-order kinetics, with the rate constant exhibiting binding-limited behavior at low association rates and reaction-limited behavior at higher rates. Implications for the rational design of effective antisense reagents are discussed.

INTRODUCTION

With increasing amounts of genome sequence data becoming available, the potential exists to use antisense oligonucleotides for the inhibition of gene expression in a wide variety of therapeutic and biotechnological applications. Antisense oligonucleotides hybridize to their target mRNA by Watson-Crick basepairing and inhibit translation of the mRNA by enzymatic and steric means (Walton et al., 2000). Traditionally, active antisense oligonucleotides have been identified by trial and error of a number (20–50) of sequences (Smith et al., 2000; Stein, 1999), and this practice continues (Andreyev et al., 2001). These methods are time-consuming and typically suffer from a low rate of success. Although the criteria for activity are somewhat subjective and depend on the system and application, most estimates are that fewer than 15% of tested oligonucleotides are active (Stein, 1999). Although extensive research has identified barriers presented by cells to oligonucleotide entry and activity, even tests outside of the context of cells do not often yield oligonucleotides with sufficient efficacy (Roth and Yarmush, 1999). Combinatorial approaches, including hybridization of a target mRNA to an oligonucleotide array and digestion of target mRNA with ribonuclease H in the presence of an oligonucleotide library, are being evaluated as a means to identify susceptible sites on the mRNA (Ho et al., 1998; Lima et al., 1997; Milner et al., 1997). Complementary efforts have focused on applying RNA and oligonucleotide structural information as a means to predict rationally those sequences that should be particularly active against a target mRNA (Smith et al., 2000).

Whereas understanding of molecular recognition in protein-protein interactions has been aided by structural information determined by x-ray crystallography and NMR, scant information is available for the understanding of oligonucleotide/mRNA interactions. In the absence of direct structural data, inferences regarding RNA structure have been derived from minimum free-energy theoretical predictions of RNA folding, which are in turn validated using indirect comparative, enzymatic, and chemical methods, in some cases also using oligonucleotides as structural probes (Eckardt et al., 1997; Jaeger et al., 1989; Lima et al., 1992, 1997; Mathews et al., 1999b; Zuker and Jacobson, 1995; Zuker et al., 1991). Several researchers have sought to use RNA structural predictions as a basis for selecting effective antisense oligonucleotides, but simple inspection of folded structure does not reveal any general relationships with antisense effectiveness. A more productive approach is to use this information in a thermodynamically consistent model, which accounts for unfolding of oligonucleotide and RNA molecules to expose bases needed for hybridization, the basepairing between the deoxyribonucleotides of the

Received for publication 3 July 2001 and in final form 29 August 2001.

Address reprint requests to Dr. Charles M. Roth, Departments of Chemical and Biochemical Engineering and Biomedical Engineering, Rutgers University, 98 Brett Road, Piscataway, NJ 08854. Tel.: 732-445-4109; Fax: 732-445-2581; E-mail: cmroth@rci.rutgers.edu.

0006-3495/02/01/366/12 $2.00

antisense molecule and the ribonucleotides of the target, and restructuring of the bound target to a new free energy minimum (Mathews et al., 1999a; Walton et al., 1999). Summing the free energies of each of these steps gives a total free energy for antisense binding to a particular sequence on a target mRNA. Predictions are then generated for many possible antisense oligonucleotides binding to particular mRNA species. To date, such predictions have been compared to several data sets, with significant correlations observed between predicted free energy and measured binding, RNase H activation, and antisense efficacy (Jayaraman et al., 2001; Mathews et al., 1999a; Walton et al., 1999). These promising results point to the role of RNA structural flexibility as a key factor in determining the accessibility of RNA to antisense binding, but highlight the importance of accounting for the whole process simultaneously. Nonetheless, there clearly exists a need for more thorough investigation, both experimental and theoretical, of the biophysics involved in the interaction of short oligonucleotides with their full-length mRNA targets.

Toward this end we chose to study the affinity and kinetics of hybridization of 17-mer oligodeoxynucleotides (ODNs) complementary to in vitro transcribed rabbit β-globin (RBG) mRNA, a well-studied mRNA found to exhibit considerable variability in both binding affinity and in vitro antisense efficacy, depending on the complementary ODN sequence chosen (Cazenave et al., 1987; Goodchild et al., 1988; Milner et al., 1997). To measure binding in solution quantitatively and rapidly, we developed an assay based on the rapid and efficient separation of free ODN from hybridized ODN by centrifugation through size-selective membranes. We used this assay to investigate the affinities and kinetics of binding of a panel of ODNs targeting regions of various character (base composition and predicted structure) on the RBG mRNA. In addition, we studied the dynamics of RBG mRNA cleavage in the presence of ODNs of varying association kinetics and a constant level of ribonuclease H, which recognizes DNA/RNA duplexes and is believed to play a significant role in the antisense mechanism in vivo. Confident prediction and measurement of hybridization affinity and kinetics will reduce the number of failure sequences tested in antisense assays and improve the likelihood of identifying those sequences that will be active most rapidly at the lowest possible concentrations.

MATERIALS AND METHODS

Oligonucleotide/mRNA hybridization free energy prediction

The method used for free energy predictions was described in detail in an earlier publication (Walton et al., 1999). Briefly, and in general terms, the energies of folding for the target mRNA and ODN were calculated using the nearest-neighbor algorithm developed by Zuker et al., *mfold* (Walter et al., 1994; Zuker, 1989). The algorithm was applied using thermodynamic parameters available with *mfold 2.3*, using the "N Best" program with a sort percentage of 10, 1 traceback, and a window size of 0, at a temperature of 37°C.

The energies of folding were used to calculate the overall free energy of antisense binding ($\Delta G^\circ_{\text{total}}$) by considering the free energies of RNA unfolding ($\Delta G^\circ_{\text{unfold}}$), the negative of which was computed by *mfold*); the corresponding energy of ODN unfolding ($\Delta G^\circ_{\text{oligo}}$), computed analogously, except with DNA rather than RNA parameters (SantaLucia et al., 1996); the free energy for the intermolecular interaction of the ODN and the mRNA ($\Delta G^\circ_{\text{hyb}}$), which was computed using nearest-neighbor parameters for DNA/RNA hybrids (Sugimoto et al., 1995); and the energy to refold the mRNA into a new minimum energy structure with the constraint of the antisense ODN bound to its complement ($\Delta G^\circ_{\text{restruct}}$). Thus, $\Delta G^\circ_{\text{total}}$ is given by the sum:

$$\Delta G^\circ_{\text{total}} = \Delta G^\circ_{\text{unfold}} + \Delta G^\circ_{\text{oligo}} + \Delta G^\circ_{\text{hyb}} + \Delta G^\circ_{\text{restruct}} \quad (1)$$

The path by which free energies are calculated (i.e., involving complete unfolding of the RNA) does not correspond to the physical situation, but the thermodynamic cycle will provide the correct total free energy, if equilibrium is truly attained. For the purposes of comparing the ability of various target regions on the mRNA to accommodate an ODN, the sum ($\Delta G^\circ_{\text{unfold}} + \Delta G^\circ_{\text{restruct}}$) is used and termed the "RNA structure cost." Because the initial RNA folded state is at its minimum free energy, the RNA structure cost is always non-negative. The $\Delta G^\circ_{\text{oligo}}$ term is likewise non-negative, though frequently zero, and the $\Delta G^\circ_{\text{hyb}}$ is always negative. Thus, there is a balance between unfavorable (costs) and favorable (gains) contributions to $\Delta G^\circ_{\text{total}}$.

ODN preparation

Phosphodiester oligodeoxynucleotides were obtained from Life Technologies (Carlsbad, CA), prepared at 200 nmol scale and purified by HPLC. Before use, the lyophilized ODNs were resuspended to 100 μM concentration in Tris-EDTA (TE, pH 8.0) buffer per the manufacturer's instructions. Before labeling, all ODNs were stored at −20°C. ODNs were 5′-labeled with ^{33}P-γ-ATP (NEN Life Science Products, Boston, MA) using T4 polynucleotide kinase (PNK) and standard forward reaction conditions (Promega, Madison, WI). Unincorporated label was removed from the reaction by separation on a Chroma-Spin 10+STE column (Clontech Laboratories, Palo Alto, CA). ODNs were then phenol-chloroform-extracted and ethanol-precipitated with ammonium acetate to ensure complete removal of PNK and any other contaminating buffer components. If necessary, an additional purification was performed using NucAway Spin Columns (Ambion, Austin, TX). ODNs were resuspended in TE and the purity verified by electrophoresis. Labeled ODNs were stored at 4°C for daily use. Position label refers to the 5′ base of the mRNA to which the 3′ base of the ODN is complementary.

cDNA preparation and in vitro transcription

The pSV2RbetaG clone was obtained from ATCC (ATCC no. 37646). The RBG encoding insert was extracted by double digestion with *Hind*III and *Bgl*II. The gel-purified insert was ligated into the pSP73 vector (Promega). The new vector was transformed into competent cells, and vector-carrying clones were selected from individual colonies growing on agar-amp50 plates. Clone 73-10-1-1 was grown into large-volume cultures, as needed, and the plasmid purified by Maxi-prep (Qiagen, Valencia, CA). The insert sequence was verified by positive and negative strand sequencing (Massachusetts General Hospital DNA Sequencing Core Facility). The plasmid was linearized using *Bgl*II, and the mRNA was transcribed with the MegaScript in vitro transcription system (Ambion), per the manufacturers' instructions. RNA was distributed into aliquots and stored at −80°C. RNA purity was confirmed by denaturing PAGE using TBE-Urea Ready Gels (Bio-Rad, Hercules, CA).

Hybridization reactions

Hybridization reactions were performed in 96-well, non-binding surface plates (Corning, Acton, MA). This minimized adsorption of the nucleic acids, which was observed when microcentrifuge tubes were used to perform the hybridizations. All hybridization reactions were performed in 1 M NaCl, 0.5 mM EDTA, and 20 mM sodium cacodylate, pH 7.0. Equilibrium hybridization reactions were performed for at least 16 h, but no more than 20 h; no differences were seen in the degree of hybridization for any of the ODNs throughout this time period. Kinetic hybridization reactions were performed at a concentration of mRNA sufficient to generate 100% binding of the ODN at equilibrium. In each case, an mRNA-containing and an ODN-alone control hybridization were performed for the same time period (see Data Analysis). ODNs were used at the minimum detectable concentration, typically within 2 weeks of the calibration date of the radioactivity. This resulted in ODN concentrations of 2–4 pM. In situations where minimum ODN concentrations were required (where the measured K_D was close to 0.01 nM), ^{33}P-γ-ATP at or before its calibration date was used to ensure maximal sensitivity.

Gel-shift separation

After hybridization, 15 μl of the hybridization reaction was added to 3 μl of 6X loading buffer (30% glycerol, 0.25% bromophenol blue, 0.25% xylene cyanole). From this mixture, 15 μl were then loaded onto a 4–20% gradient acrylamide gel and electrophoresed until the bromophenol blue front reached ~75% of the length of the gel. The location of the mRNA was verified using SYBR Gold nucleic acid gel stain (Molecular Probes, Eugene, OR). Gels were then dried on Whatman filter paper at 80°C for 45 min under vacuum. The dried gels were exposed to imaging screens for 40 h, and accumulated signal from ^{33}P-γ-ODN was measured using the Molecular Imager (Bio-Rad). Band densities were quantified using the Multi-Analyst software package (Bio-Rad). The fraction bound was calculated as the signal in the band corresponding to bound ODN divided by the total signal of the bound and free bands.

Centrifugal separation

After hybridization, 100 μl of the hybridization reaction was loaded onto a Microcon-50 centrifugal concentrator (Millipore, Bedford, MA). The concentrators were loaded into an Eppendorf 5415C centrifuge and centrifuged for ~40–60 s at 8200 × g (10,000 rpm). The membranes were then inverted into a new centrifuge tube and centrifuged for ~20 s at 10,000 rpm. The initial centrifuge time was adjusted to generate a permeate fraction of ~50% of the added volume. The volumes in each fraction were measured using a micropipette, and each fraction was counted by liquid scintillation (counter: Beckman 6000IC; fluid: Ultima Gold, Packard Biosciences, Meriden, CT). To ensure that a constant concentration of ODN was added to each reaction and that the retentate was fully recovered from the membrane, the radioactivity on the separator membrane was also measured.

RNase H cleavage experiments

Ribonuclease H cleavage experiments were performed in a buffer suitable for maintaining enzymatic activity: 0.1 M KCl, 10 mM $MgCl_2$, 1 mM DTT, and 50 mM Tris-HCl (pH 8.0). The hybridization buffer (i.e., 1 M NaCl) eliminated enzyme activity and could not be used. ODN and mRNA were each used at a concentration of 50 nM. Equilibrium and kinetic hybridization experiments were performed under these conditions with selected ODNs to ensure that equivalent K_D and k_a values were achieved in the RNase H and hybridization buffers (data not shown). Three units of RNase H was added to the ODN solution, after which RNA was added and an initial sample taken, defining time 0. Subsequently, six aliquots were taken at various times and added to formamide-containing gel-loading buffer to stop the cleavage reaction. The samples were then run on a 10% TBE-Urea Ready Gel (Bio-Rad) and post-stained using SYBR Gold nucleic acid gel stain (Molecular Probes). Fluorescence was measured using the Fluor-S system and quantitated using the Multi-Analyst software package (Bio-Rad). The band intensities were expressed as a fraction of the maximum measured band intensity (maximum amount of cleaved product) to normalize for differences in staining and exposure.

Data analysis

After centrifugal separation, the radioactivity (cpm) and volume of each fraction were measured. Two key principles are necessary to quantify the fraction of ODN bound to mRNA from these measurements. First, the permeate fraction is assumed to contain only free ODN, while the retentate contained free ODN and any bound ODN. This assumption was verified by electrophoresis. Therefore, the (radioactive) label in the retentate (R) and permeate (P) is distributed as

$$R = R_{\text{bound}} + R_{\text{free}} \tag{2}$$

$$P = P_{\text{free}} \tag{3}$$

where the subscripts "bound" and "free" refer to the state of the ODN. Second, the separation is assumed to occur rapidly, such that dissociation of bound hybrids does not occur during the separation. The concentrations of free ODN in the retentate and permeate after centrifugal separation are then assumed to be related by a membrane distribution coefficient, K_{memb}:

$$K_{\text{memb}} = \frac{[\text{free oligo}]_{\text{retentate}}}{[\text{free oligo}]_{\text{permeate}}} = \frac{R_{\text{free}}/V_R}{P/V_P}, \tag{4}$$

where V_R and V_P are the volumes of the retentate and permeate fractions, respectively. The value of K_{memb} is determined experimentally in each sequence of measurements on a labeled ODN sample in the absence of RNA. This quantity reduces to unity if the concentrations in each fraction are exactly equal, as should be the case for a membrane pore size much larger than required for the ODN. Indeed, the measured values of K_{memb} ranged from 0.95 to 1.10. For kinetic experiments, the K_{memb} was measured for each distinct time point, though no variation was observed with time.

The fraction of bound ODN (in the hybridization reaction, before separation) is given by:

$$f = \frac{R_{\text{bound}}}{R + P} \tag{5}$$

Combining Eqs. 2–5 provides the expression used to determine fraction bound, in terms of measured quantities:

$$f = \frac{R - V_R(P/V_P)K_{\text{memb}}}{R + P} \tag{6}$$

The equilibrium dissociation constant, K_D, for the binding of each ODN to the RBG mRNA (at total concentration M_T) was determined by applying a mass action law. The data reported were calculated by fitting the fraction bound data to:

$$f = \frac{M_T}{M_T + K_D} \tag{7}$$

Fits were made to composite data sets for at least two independent experimental runs, resulting in a total of 12–25 data points per K_D value. It is assumed that the concentration of free mRNA remains unchanged throughout the experiment. Since this requires the mRNA concentration to be

substantially greater than the ODN concentration (the practical minimum for which was ~2 pM), we estimate that the lower limit on the range of measurable K_D values is ~0.005–0.010 nM. To ensure an accurate fit, fraction-bound data were normalized to 100% by dividing by the maximum measured fraction bound (typically 0.96–0.98) before being fit by Eq. 7.

Kinetic data were fit using a second-order rate law for the formation of duplexes (D) from ODNs (O) and mRNA (M). As in the equilibrium experiments, it was assumed that mRNA concentration remains unchanged over time, such that a pseudo-first order condition occurs:

$$\frac{dD}{dt} = k_a OM - k_d D \cong k'_a O - k_d D \tag{8}$$

where k_a is the second-order association rate constant, k_d is the first-order dissociation rate constant, and the pseudo-first order rate constant, k'_a, is equal to $k'_a = k_a M_T$. Applying the condition $k_d = K_D k_a$, imposing an initial condition of no bound ODN, and solving for fraction bound gives:

$$\frac{f}{f_{eq}} = 1 - e^{-k_{fit}t} \tag{9}$$

where f_{eq} is the equilibrium value given by Eq. 7, and k_{fit} is given by:

$$k_{fit} = \frac{k'_a}{f_{eq}} = \frac{k_a M_T}{f_{eq}} \tag{10}$$

Therefore, the fraction bound was measured over a range of times during two independent experimental runs, the composite data fit to Eq. 9, and the second-order association rate constant, k_a, determined using Eq. 10.

The cleavage of RNA by ribonuclease H in the presence of antisense ODN was observed to follow first-order kinetics, as can be derived from mechanistic arguments (see the Appendix). Because the appearance of cleavage product could be quantified more accurately than the disappearance of full-length RNA, the former was used and fit to an equation of the form:

$$X = 1 - e^{-k_{eff}t} \tag{11}$$

where X is the fractional increase in cleavage product and k_{eff} is the effective first-order rate constant.

All data fits were performed using Kaleida Graph software (Synergy Software, Reading, PA).

RESULTS

To date, a paucity of experimental data exists regarding the interactions between antisense oligonucleotides and their complementary, but structured, messenger RNAs in solution. To measure the binding of an oligonucleotide to its target mRNA, it is important to be able to separate hybridized oligonucleotides from free. Traditionally, this is accomplished with a gel-mobility shift assay. However, limited sample volumes and constraints of usable buffers make this technique relatively inflexible. We have adopted a centrifugal separation method designed to separate bound oligonucleotides from free in a faster, more quantitative, and more sensitive fashion than the gel-shift assay. The basic premise of the assay is to perform a rapid separation, such that free oligonucleotides pass through a semi-permeable membrane, while bound oligonucleotides are prevented from permeating due to the size of the RNA to which they are bound; the fraction bound is then computed from measurements of label in each compartment with equilibrium and mass balance relationships (see Materials and Methods).

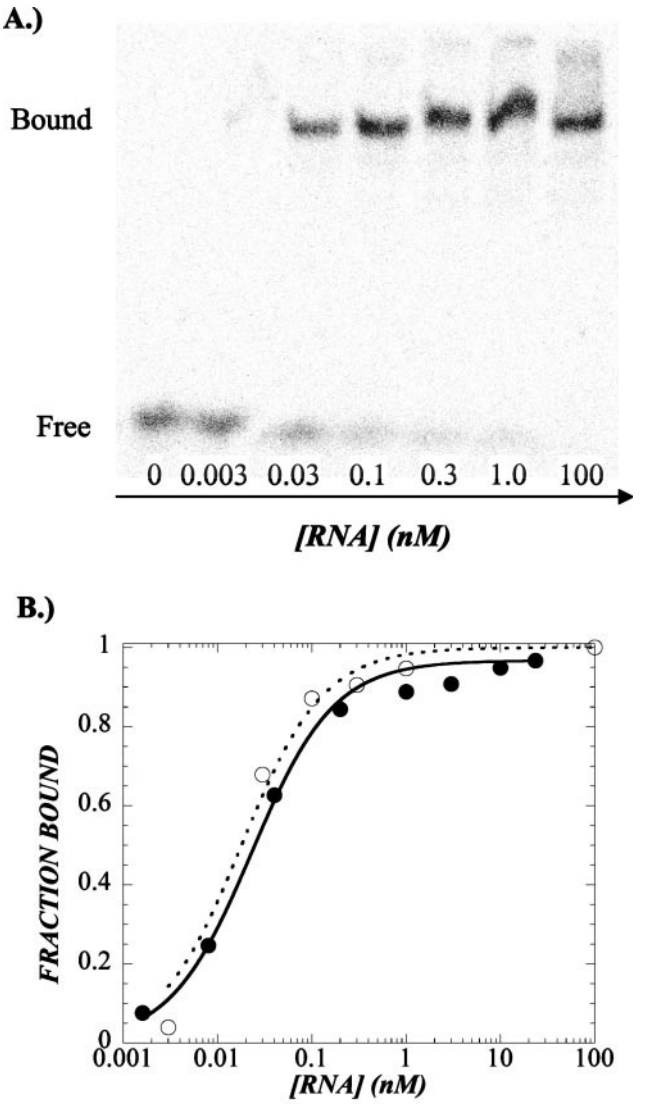

FIGURE 1 Comparison of oligonucleotide binding between gel-shift and centrifugal assays. (*A*) Radiographic image of a 4–20% gradient polyacrylamide gel showing bound and free oligonucleotide with increasing concentration of RBG mRNA. (*B*) Fraction of oligonucleotide bound as measured by each assay versus free mRNA concentration (assumed unchanged from initial concentration). Data points normalized to maximum binding, typically 96–98% (see Methods). (●) Gel-shift assay; (○) centrifugal assay. Curves show the fits of Eq. 7 to each of the data sets. The K_D values obtained from curve fits are given in Table 1.

After verifying that oligonucleotides completely permeated and that the RBG mRNA was completely rejected by the membrane under use, we compared the binding curves measured with the centrifugal separation technique with those from a gel-shift assay. Fig. 1 *A* shows a typical gel-shift assay using a 17-mer phosphodiester oligodeoxynucleotide (ODN) targeting position 259 on the RBG

mRNA (in this paper, we refer to position as the 5′-end of the mRNA, thus, 3′-end of the ODN). In the gel-shift assay, radiolabeled ODN that is bound to RNA experiences a decrease in electrophoretic mobility and is retained at the top of the gel. As expected, with increasing mRNA concentration, the quantity of radioactivity in the bound fraction increases. The fraction bound was calculated from the band intensities and compared with the binding curve measured for the same ODN-mRNA interaction using the centrifugal separation assay (Fig. 1 *B*). The slight (log scale) discrepancy between the two methods was consistent for a range of binding curves, with the centrifugal technique reporting higher K_D values (by a factor of 1.2–3). The slightly higher K_D values for the centrifugal assay could reflect incomplete equilibration between the retentate and permeate (though our results in the absence of mRNA suggest this is unlikely) or the difference in buffer conditions used for the gel-shift assay, where the samples were mixed with loading buffer before electrophoresis.

Next, we used the centrifugal assay to study the binding of a panel of ODNs complementary to the RBG mRNA. These included a selection of those previously studied in an oligonucleotide array (Milner et al., 1997) and several more chosen to provide a diversity of predicted affinities and predicted structural characteristics. A range of K_D values spanning nearly five orders of magnitude was accessible with this binding assay (Table 1). As a control, we also measured the binding curves for several nonsense ODNs, which are identical in base composition to their antisense counterparts but are in scrambled sequence, and hence should not hybridize to their target. Indeed, binding was not observed for nonsense sequences corresponding to ODNs 33, 58, 59, 103, and 107 at the highest tested mRNA concentration, confirming the requirement of sequence complementarity for binding of ODNs to their target mRNA.

Also listed in Table 1 are the K_D values calculated from the free energies of binding predicted with our molecular thermodynamic model (see Methods and Walton et al., 1999). Although not in quantitative agreement with measured values, the predictions generally distinguish between ODNs with large differences in affinity. When the predicted affinity values are ranked and assigned a percentile score (the sequence of highest affinity is at 100 and the median is 50), this score correlates fairly well with measured affinity (Fig. 2 *A*). When examining those ODNs with measured K_D values <0.1 nM, in only one case was the percentile score <78, with two of these ODNs scoring at greater than the 98th percentile. From these results, we infer that using model predictions as a means to select high affinity ODNs is likely to result in a fraction of false positives and false negatives, but overall should reduce significantly the number of sequences to be tested.

Previously, the loci of binding of labeled RBG mRNA were determined by exposure to an ODN array on which were immobilized all antisense sequences, up to 17 nucleotides in length, spanning the first 121 bases of the particular RBG transcript used (Milner et al., 1997). The results were reported for each ODN in terms of a radiographic intensity, roughly proportional to amount bound, which ranged from ~11 to 1000 arbitrary intensity units, with a mean intensity of ~150. In the array experiment, an mRNA concentration of 0.1 nM was used. Because of the relationship between fraction bound and dissociation constant (Eq. 7) the array experiment probably only distinguishes among equilibrium dissociation constants in the range $0.01\ \text{nM} < K_D < 1.0$ nM. In comparing nine ODNs whose binding was measured by each assay, a general correlation is observed between equilibrium dissociation constant and binding intensity (Fig. 2 *B*). In general, the highest-affinity ODNs in our measurements correspond to those exhibiting high binding in the array format, though the more limited dynamic range of the latter prevents a solid quantitative comparison.

The kinetics of ODN binding to target mRNA may also be quite important in antisense applications. The dynamics of delivery and degradation dictate that ODNs must not only bind with sufficient affinity, but also with sufficiently rapid kinetics to have an effect in living cells. To determine the

TABLE 1 Equilibrium binding of oligonucleotides to the RBG mRNA at 37°C

Target Position	Measured K_D (nM)	Predicted K_D (nM)	Percentile*
58	0.011 ± 0.001	0.0014	84
59	0.012 ± 0.002	0.010	78
49	0.015 ± 0.002	2.1×10^{-5}	98
259	0.019 ± 0.002	0.0024	82
84	0.021 ± 0.002	0.0062	79
79	0.031 ± 0.004	15	30
139	0.072 ± 0.006	3.6×10^{-6}	99
448	0.10 ± 0.02	2.4×10^{-4}	92
438	0.22 ± 0.02	7.8×10^{-5}	95
217	0.22 ± 0.02	0.11	62
107	0.54 ± 0.07	1.8	42
33	1.1 ± 0.3	4.8	34
98	2.7 ± 0.4	200	22
147	7.3 ± 0.9	2.9×10^{-4}	91
103	310 ± 30†	240	21
407	550 ± 50†	>10000	2
33Non	≫150	N/A‡	
58Non	≫150	N/A‡	
59Non	≫150	N/A‡	
103Non	≫150	N/A‡	
107Non	≫150	N/A‡	

*Rank of predicted affinity of 494 sequences. An oligonucleotide with the highest predicted affinity would have a percentile score of 99, i.e., the oligonucleotide would be in the 99th percentile.

†Extrapolated values, based on the fractional binding curve at mRNA concentrations <150 nM. For nonsense sequences no extrapolation could be made, as no measurable binding was detected at any concentration tested.

‡No value could be predicted, as no specific binding interaction could be defined.

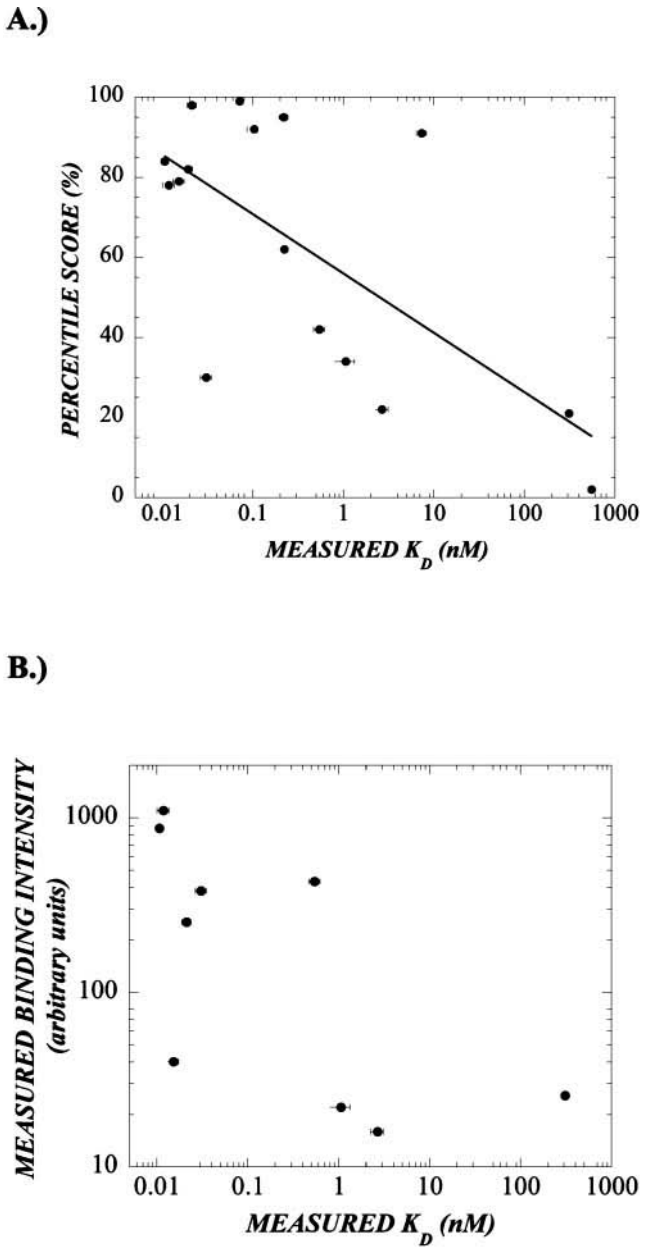

FIGURE 2 Equilibrium dissociation constant correlations. (*A*) Correlation of percentile score (see text for definition) from thermodynamic binding affinity predictions with measured K_D values. Error bars represent the uncertainty for the nonlinear fit of each K_D value based on a composite data set of 12–25 points each. The line is the logarithmic curve fit to the data with the equation $y = -14.5\log(x) + 56.7$; $R^2 = 0.44$. (*B*) Correlation of solution-phase binding affinity measurements with binding intensity of RBG mRNA to a solid-phase oligonucleotide array. Binding intensity data were obtained from Milner et al. (1997) and are in arbitrary units.

role of mRNA structure in controlling the hybridization kinetics, eight ODNs with varying predicted RNA structure costs and energetic gains, but generally intermediate affinities (as we found these were most amenable to accurate kinetic determination) were chosen for kinetic study. Association kinetics for each of these ODNs were measured using the centrifugal assay for a number of time points leading up to equilibrium. Because the RNA concentration was much greater than the ODN concentration, the fraction bound versus time profiles followed pseudo-first-order behavior (Fig. 3 *A* and Eq. 9), from which second-order rate constants were obtained with knowledge of the RNA concentration and equilibrium fraction bound (Eq. 10). For all of the ODNs studied, the association rate increased with temperature. Because duplex stability decreases with temperature, the increase in k_a with temperature can be interpreted as the decrease in intramolecular RNA basepairing, thus making target sites more accessible to hybridization by ODN. The rate constants appeared to obey an Arrhenius law over the temperature range studied, although not enough data points were generated to obtain accurate values for the activation energy (Fig. 3 *B*).

Second-order association rate constants were found to correlate strongly with overall affinity (Fig. 4), and the values are similar to those measured in previous studies of ODN hybridization (Patzel et al., 1997; Schwille et al., 1996). Because of the correlation between the association rate constant, k_a, and equilibrium dissociation constant, K_D, the dissociation rate constant, k_d ($=k_aK_D$), is relatively constant for almost all of the ODNs studied (Table 2). The one exception is ODN 33, which exhibited unusually rapid association kinetics. RNA folding calculations suggest that this might be explained by the very low energetic cost of altering the RNA structure, combined with no cost for altering the ODN structure (i.e., no hairpins or other stable secondary structures are formed).

The importance of RNase H in the action of antisense oligonucleotides in cell culture is well-established (Helene and Toulme, 1990). To understand the relationship between the kinetics of hybridization and the dynamics of RNase H-mediated cleavage of ODN/mRNA duplexes, hybridization experiments were performed in the presence of RNase H at 37°C. As can be seen for ODNs 139 and 147, cleavage by RNase H results in the formation of two bands corresponding in each case to the length of the regions upstream and downstream of the target site of the ODN (Fig. 5). For all ODNs tested, the appearance of cleavage product was described by first-order kinetics, but complete degradation was never observed, possibly due to loss of enzyme activity or product inhibition. The effective rate constants for RNase H cleavage, k_{eff}, are listed in Table 2. Although there is some scatter, the k_{eff} values are relatively insensitive to the association rate constants, except at low values of k_a (Fig. 6); this behavior is predicted by the putative reaction scheme (see the Appendix) and corresponds to binding-limited and reaction-limited cases at low and high k_a, respectively.

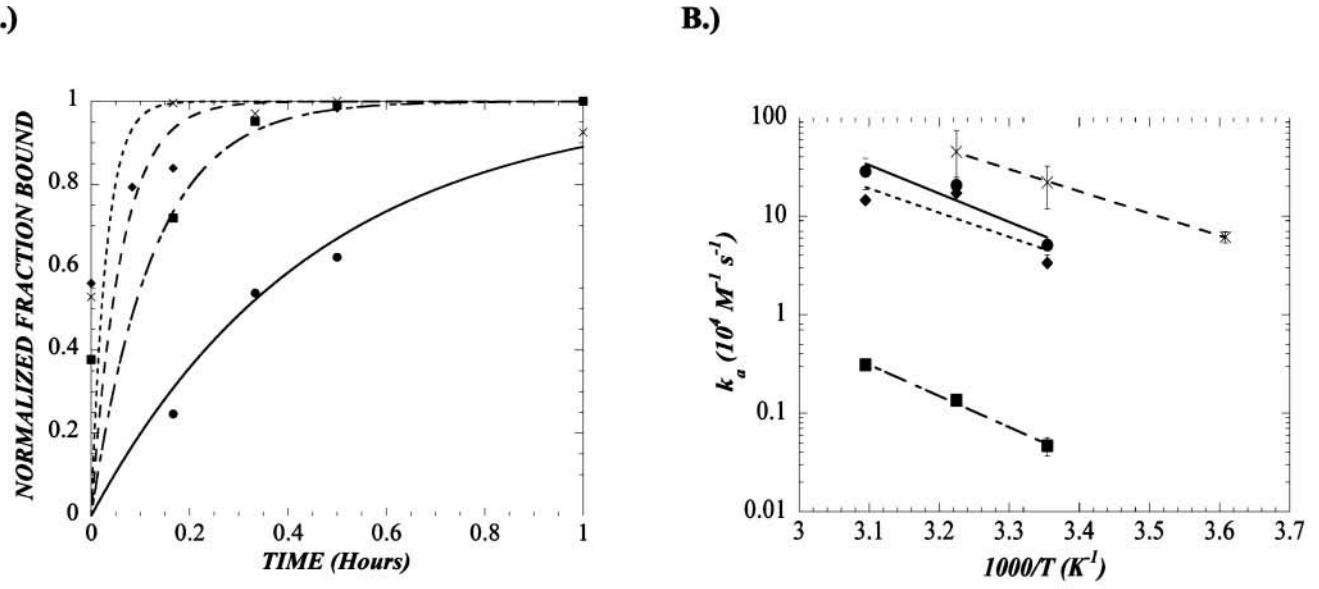

FIGURE 3 Kinetics of hybridization vary with temperature. (*A*) Kinetics of hybridization are shown for oligonucleotide 259 binding to the RBG mRNA at (●) 4°C, (■) 25°C, (◆) 37°C, and (×) 50°C. Curves represent the fits to Eq. 9. (*B*) Arrhenius plot for oligonucleotides (●) 139, (■) 147, (×) 259, and (◆) 448.

DISCUSSION

There has been relatively little study of the interactions between long mRNA molecules (500–4000 nt) and short oligonucleotides (12–25 nt). In mechanistic studies of hybridization, such as those from which nearest-neighbor parameters are determined, short oligonucleotides (typically 6–8 nt) of similar length have been used (Bommarito et al., 2000; Mathews et al., 1999b). This situation is quite different from that for antisense hybridization, where a highly structured mRNA hybridizes with a minimally structured and much shorter oligonucleotide. The selection of hybridization site becomes critical, as each oligonucleotide encounters a different structural landscape on the mRNA. Using a quantitative assay of binding in solution, we have shown that a panel of 17 nt ODNs complementary to the RBG mRNA exhibits affinities (or, equivalently, equilibrium dissociation constants) spanning nearly five orders of magnitude. Furthermore, for ODNs targeting regions overlapping by as many as 13 of 17 nt, affinity can vary over 100-fold (e.g., Table 1, ODNs 103 and 107). Similarly, association rate constants were found to vary over several orders of magnitude, and in general these mirror the variation in affinity. It is to be expected that such drastic differences in affinity and association kinetics will lead to the types of variability in antisense efficacy often seen in the data from ODNs selected randomly from the target sequence, even if the search is constrained to a small region of the target mRNA.

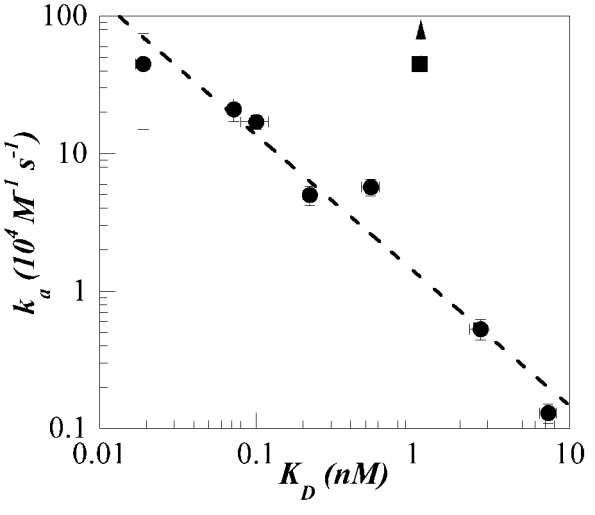

FIGURE 4 Correlation of association rate constant with equilibrium dissociation constant. Second-order association rate constants and equilibrium dissociation constants were determined as described in the text for a panel of oligonucleotides targeting regions of the RBG mRNA with varying predicted structural characteristics. The dotted line is the power law regression: $\log(k_a) = \log(1.4) - 0.985 \log(K_D)$ ($R^2 = 0.940$). The square symbol and arrow represent oligonucleotide 33, for which binding was very rapid, and k_a could only be bounded.

One approach to identify high-affinity antisense oligonucleotides is hybridization of mRNA to an array of immobilized antisense sequences (Milner et al., 1997; Mir and Southern, 1999). Our results for affinity of ODNs complementary to RBG generally correlate with oligonucleotide array measurements (Fig. 2 *B*), with some of the discrepancies likely due to the limited dynamic range of the latter approach. Specifically, the ODN in the lower right corner of Fig. 2 *B* appears to be uncorrelated, but this is because its

TABLE 2 Predicted thermodynamics and measured thermodynamics and kinetics for ODNS complementary to the RBG mRNA at 37°C

Target Position	Total Energy (ΔG°_{total}, kcal/mol)	RNA Structure Cost ($\Delta G^\circ_{unfold} + \Delta G^\circ_{restruct}$, kcal/mol)	Oligonucleotide Structure Cost (ΔG°_{oligo}, kcal/mol)	Intermolecular Hybridization Gain (ΔG°_{hyb}, kcal/mol)	K_D (nM)	k_a (10^4 $M^{-1} \cdot s^{-1}$)	k_d^* (10^{-5} s^{-1})	RNase H k_{eff} (10^{-4} s^{-1})
259	−16.5	8.8	1.4	−26.7	0.019 ± 0.002	45 ± 30	0.87	4.6 ± 0.9
139	−20.5	8.8	0	−29.3	0.072 ± 0.006	21 ± 4	1.5	4.1 ± 1
448	−17.9	2.6	0.9	−21.4	0.10 ± 0.02	17 ± 2	1.8	3.0 ± 0.3
438	−18.6	5.4	0.7	−24.7	0.22 ± 0.02	5.0 ± 0.8	1.1	3.8 ± 0.5
107	−12.4	13.4	1.2	−27	0.54 ± 0.07	5.7 ± 0.8	3.1	1.8 ± 0.4
33	−11.8	2.7	0	−14.5	1.1 ± 0.3	>45†	>50	6.5 ± 2
98	−9.5	14.2	0.9	−24.6	2.7 ± 0.4	0.53 ± 0.09	1.4	0.48 ± 0.05
147	−17.8	11.3	2.1	−31.2	7.3 ± 0.9	0.13 ± 0.02	0.99	0.47 ± 0.07

*Estimated from measured K_D and k_a values.
†Kinetics too rapid for accurate correlation; listed as higher than the highest value that was reliably measured.

binding intensity in the array format is in the background. Another cause of variation could be due to altered mRNA structure resulting from somewhat different 5′ and 3′ sequences of the in vitro transcript used in the solid phase assay versus that used in our measurements. This could be particularly important for ODN 49 (the point in the lower left quadrant of Fig. 2 *B*), whose target sequence is predicted to interact with the 5′ end of the transcript used in the array assay, but not in the transcript used in the present study. Differences could also be due to slight variations in the hybridization buffers and temperatures used, or to enhanced oligonucleotide/oligonucleotide interactions in the context of the solid phase.

We and others have found that thermodynamic prediction of the binding affinity of ODNs for their target mRNAs increases the likelihood of finding antisense sequences of high affinity, ribonuclease H activity, and efficacy in cell culture (Jayaraman et al., 2001; Mathews et al., 1999a; Walton et al., 1999). In this paper, thermodynamic predictions, which correspond to free solution conditions under 1 M NaCl, were tested directly with experimental measurements made under comparable conditions. The range of dissociation constants observed experimentally ($0.01 \leq K_D \leq 550$ nM) was significantly smaller than the range predicted from the model ($4 \times 10^{-6} \leq K_D \leq 10^4$ nM), though for a number of ODNs the predictions were indeed of the right order of magnitude (Table 1). In light of the unrealistically wide range of predicted dissociation constants, it seemed more reasonable to express the predictions as a ranking, or percentile score, which indicates those ODNs that should have lower and higher affinity on a relative scale. On this basis, there is a positive correlation with solution binding affinity (Fig. 2 *A*), but the correlation is of moderate power, similar to comparisons of our predictions with binding measured by an ODN array (Walton et al., 1999), or with ribonuclease H susceptibility (Mathews et al., 1999a) and activity in cell culture (Jayaraman et al., 2001). Taken together, these results suggest that the limitation in using binding affinity predictions to select antisense reagents is not the difference in binding in solution versus in cells (Matveeva et al., 1998) or the sequence-dependent

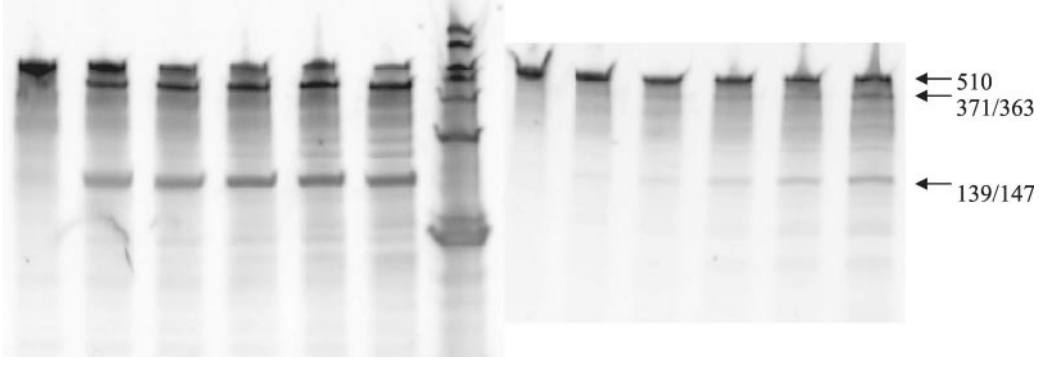

FIGURE 5 Kinetics of RNase H cleavage by oligonucleotides 139 and 147. Typical RNase H cleavage pattern showing the full-length mRNA (510 nt), and the two cleavage products (139 nt, 371 nt, *left*; 147 nt, 363 nt, *right*). In each case the lanes from left to right represent time points of 0, 15 min, 30 min, 1 h, 2 h, 4 h. Markers (from bottom) 100, 200, 300, 400, 500, 750, 1000 nt. First-order initial cleavage rate constants, k_{eff}, obtained from the fits of the data to Eq. 11, are shown in Table 2.

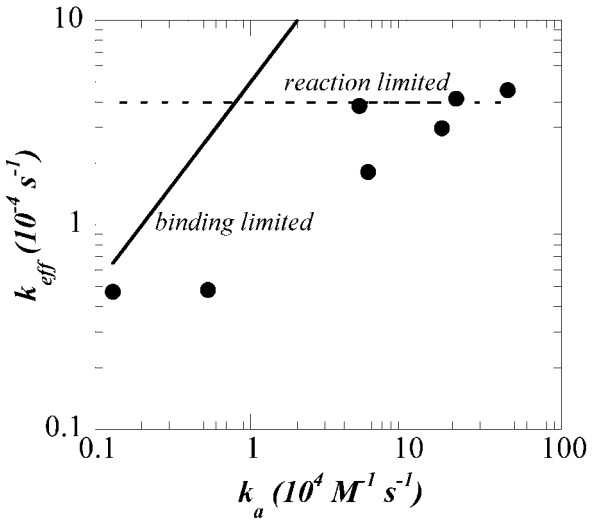

FIGURE 6 Correlation of ribonuclease H cleavage with oligonucleotide association to the RBG mRNA. The association rates and RNase H cleavage kinetics were measured for a panel of antisense oligonucleotides. The solid line represents the expected variation in k_{eff} in the binding-limited regime (Eq. A6, no adjustable parameters), and the dotted line represents a constant k_{eff} in the reaction-limited regime (Eq. A10, with the maximum fit to the data at the three highest k_a values.

processing of ODNs by cells, but the imperfect ability to predict affinity itself.

Binding affinity predictions are limited by the accuracy of structural descriptions. In structural prediction alone, 70–80% accuracy as compared to phylogenetically determined structures is sufficient to predict the major features of the native mRNA structure (Mathews et al., 1999b). However, when looking at ODNs that might target at most 5% of the mRNA structure (e.g., a 25-mer targeted to a 500 nt mRNA), greater accuracy will be required to increase the reliability of oligonucleotide hybridization energy predictions. Efforts to extend these predictions have focused on predicting pseudoknot formation and combining free energy predictions with other methods, such as a comparative analysis or statistical sampling (Ding and Lawrence, 2001; Juan and Wilson, 1999; Rivas and Eddy, 1999; Tabaska et al., 1998). However, the lack of detailed experimental data with which to validate folding algorithms is likely to limit the development of major improvements in the near future.

When secondary structural features can be more accurately predicted and tertiary interactions can be accurately modeled and understood (Wu and Tinoco, 1998), it will be possible to further reduce the fraction of ODNs that should be tested in vitro to be considered viable antisense candidates. For the time being, predictions of binding affinity will be useful in concert with accurate in vitro assays. A useful metric for rational selection may be the percentile score (Fig. 2 *A*). For example, the group of ODNs measured to have K_D values <0.1 nM had average percentile scores of 79%. For the 0.1–1.0 nM and >1.0 nM groups, respectively, the average scores are 73% and 34%. Selection of potential candidates from among the set expected to be highest in affinity will considerably enhance the likelihood of identifying sequences that have high affinity and are expected to have antisense activity (Matveeva et al., 1998). For example, we have experienced marked success testing in vitro sequences selected from the highest percentile scores ($>95\%$) (Jayaraman et al., 2001).

Because of the molecular rearrangements required for antisense binding, it is plausible that kinetic barriers may exist that limit the applicability of thermodynamic models. Although we have found that the calculated free energy of binding is a better predictor of binding affinity than the RNA structure alone, or the free energy of folding the RNA into its structure, one might expect the structure itself to be more indicative of association kinetics. The predicted structure of the RBG mRNA is shown in Fig. 7, with the highlighted regions representing those targeted by ODNs used in the kinetics experiments. In general, the ODNs that exhibited the most rapid binding kinetics (33, 259, 139, and 448) target regions with less structure than those exhibiting slower kinetics. ODN 33 exhibited unusually rapid binding relative to its affinity (Table 2). This ODN targets a region spanning a bulge and a joint in the RBG RNA, with several noncanonical basepairs included among the structured region in between; the energetic manifestation is that this ODN targets a region with the lowest RNA structure cost of any studied (Table 2). Thus, the RNA structure cost, while an energetic quantity, may be relevant for describing kinetic binding phenomena. Others have posited that unstructured regions of the RNA should provide necessary accessibility for oligonucleotide binding (Ding and Lawrence, 2001; Sczakiel et al., 1993), and this has been shown nicely in a case where the target was carefully genetically engineered (Vickers et al., 2000). One study of the correlation between predicted structure and cell culture effectiveness (Patzel et al., 1999) suggests that an unstructured 5′ end of the RNA is particularly important for initiating hybridization.

Kinetic effects, such as a bias toward nucleation from one side of the ODN (Patzel et al., 1999), could complicate thermodynamic prediction of ODN/mRNA affinity, but the close correlation between association kinetics and affinity suggests that this is probably not a serious limitation. Other effects could alter the agreement between theoretical prediction and experimental observation of affinity. For example, it has been suggested that a single minimum free energy structure may not accurately describe RNA and, instead, an ensemble of structures should be evaluated (Mathews et al., 1999a; Scherr et al., 2000). We have found that an ensemble-average free energy is no better a predictor of binding affinity in the RBG system (unpublished results), but qualitative use of structural ensembles has been shown to exhibit moderate utility in identifying accessible binding sites on the RBG mRNA (Ding and Lawrence, 2001).

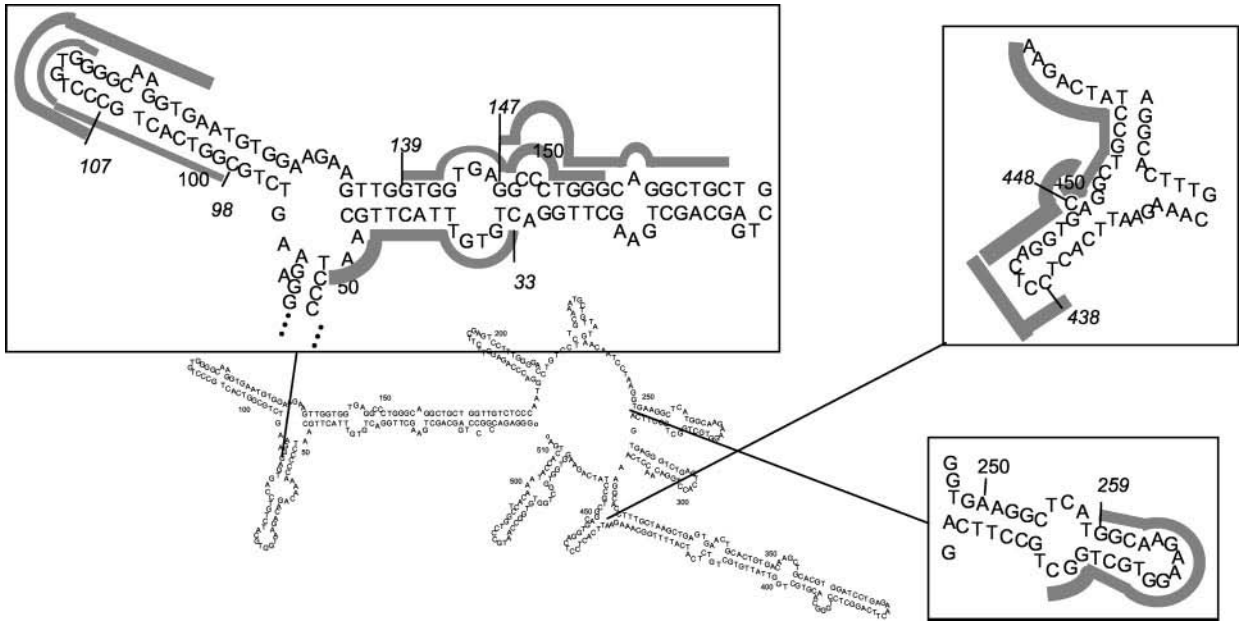

FIGURE 7 Predicted RBG mRNA structure. The predicted structure of the RBG mRNA was determined using *mfold*, as described in Materials and Methods. The complementary region for each oligonucleotide on which kinetic experiments was performed is indicated by a gray bar.

The thermodynamic model for antisense binding results in calculation of the binding affinity for an ODN/mRNA interaction under conditions that may or may not be relevant for antisense efficacy in cells. In the latter case, activity is complicated by the need for rapid kinetics, possible differences in binding thermodynamics and kinetics in the cellular environment (e.g., presence of RNA binding proteins), and the role of ribonuclease H in mediating destruction of targeted transcripts in living cells. The interplay among these different events and phenomena has not been explored extensively and quantitatively. We have sought to connect prediction of dissociation constants with their measurement, and measured dissociation constants (K_D) with association rate constants (k_a), and association rate constants with RNase H cleavage (k_{eff}). A very strong correlation was observed between K_D and k_a, with the notable exception of ODN 33, as discussed above.

A relationship between RNase H cleavage and ODN/RNA association rate is also indicated by our results. Kinetic analysis of the interplay between ODN/RNA binding and RNase H-catalyzed cleavage of duplexes shows that in the binding-limited case, the effective rate constant is equal to the product k_aO_T (see the Appendix). For the lowest values of k_a measured, the corresponding values of k_{eff} appear to approach this limit (Fig. 6 and Table 2). In the other limit of slow catalysis, the observed cleavage rate is expected to be independent of k_a (see the Appendix). Indeed, this was observed (Fig. 6), although it was necessary in this case to fit the maximum value of k_{eff}.

In vitro RNase H assays can be reliable predictors of antisense efficacy in living cells. Antisense oligonucleotides that induce cleavage of a target RNA in the presence of RNase H have been found by several researchers to be effective antisense reagents in cell culture (Ho et al., 1998; Matveeva et al., 1997). In RNase H mapping experiments the amount of both ODN and RNA is quite high, resulting in a high rate of binding, and perhaps increasing the number of ODNs that mediate cleavage. However, many antisense targets in vivo are transcripts expressed in relatively low abundance, which will present a much more stringent condition to the association of ODNs; thus, controlling the ODN library concentration may help select for the fastest binding members. It is not yet clear whether measured affinity, binding kinetics, or RNase H cleavage rates correlate most strongly with effectiveness in cell culture.

The optimization of antisense efficacy with minimal nonspecific effects will result from concerted efforts in oligonucleotide chemistry, delivery, and target site selection. With the ability to predict high-affinity sequences that bind with rapid association kinetics, it is possible to optimize the target site selection so that downstream modifications and conjugations can be explored with the greatest likelihood of success. Modifications that destabilize native mRNA structure may prove a fruitful avenue for enhancing antisense efficacy, as structural factors appear to determine which ODNs have the highest binding affinities. With the coupled dynamics of nuclease degradation and intracellular diffusion acting as kinetic traps for the effectiveness of antisense ODNs, the ability of an ODN to access its target site becomes even more critical to its activity. Although further exploration of these effects in vivo is required, it may become increasingly possible to rationally engineer highly

effective antisense ODNs for therapeutic and other applications.

APPENDIX

We found experimentally that the rate of cleavage product formation in RNase H assays followed first-order (exponential) kinetics. This rate is dependent on an interplay between association and dissociation of oligonucleotide/RNA duplexes and the kinetics of recognition and cleavage of duplexes by the ribonuclease H enzyme. Here, we present an analysis of the functional dependence of cleavage product formation under two regimes: binding-limited and RNase H-limited. In each case we seek to find how the apparent first-order rate constant depends on measurable parameters of the oligonucleotide/RNA interaction.

We consider, in general, the reaction scheme:

$$O + M \underset{k_d}{\overset{k_a}{\rightleftharpoons}} D \xrightarrow[(K_M,k_{cat})]{E} X + O \tag{A1}$$

where O is the oligonucleotide, M is the mRNA, D is the duplex that they form with association rate constant k_a and dissociation rate constant k_d, and X is the RNA cleavage product, which is formed in the presence of RNase H enzyme, E, with Michaelis-Menten parameters K_m and k_{cat}. Under the experimental conditions used, the total concentrations of oligonucleotide and mRNA, O_T and M_T, are each 50 nM; as a result, no simplification based on molar excess can be made. We consider two cases:

Case 1: binding-limited (catalysis ≫ binding)

If the rate of association is slower than catalysis, so must be the rate of dissociation, so the reaction network is essentially:

$$O + M \overset{k_a}{\longrightarrow} D \xrightarrow[(K_M,k_{cat})]{E} X + O. \tag{A2}$$

In this sequence, RNA is removed only by association with oligonucleotide, which is regenerated during the catalysis step, resulting in a first-order decay on mRNA:

$$M = M_T e^{-k_a O_T t}. \tag{A3}$$

Since the duplex is rapidly recognized by ribonuclease H and converted into RNA cleavage product and regenerated DNA oligonucleotide, the quasi-steady-state approximation applies on D:

$$\frac{dD}{dt} = k_a OM - \frac{k_{cat}E_0 D}{K_M + D} = 0. \tag{A4}$$

This equation is simplified because, under the experimental conditions, $D \ll K_M$. Solving for D and combining with Eq. A4 and the mass balance, $M_T = M + D + X$ gives an approximate profile for X, valid subject to the aforementioned approximations at times after the quasi-steady state is established

$$\frac{X}{M_T} = 1 - \left(1 + \frac{k_a O_T}{k_{cat}E_0/K_M}\right) e^{-k_a O_T t}. \tag{A5}$$

Thus, first-order kinetics are expected, with an effective rate constant

$$k_{eff} = k_a O_T. \tag{A6}$$

The total concentration of oligonucleotide was fixed at 50 nM for all of the RNase experiments performed here. Therefore, the line corresponding to Eq. A6 is shown in Fig. 7.

Case 2: reaction-limited (binding ≫ catalysis)

We begin with the rate equation for the formation of cleavage product:

$$\frac{dX}{dt} = \nu = \frac{k_{cat}E_0 D}{K_M + D} \approx \frac{k_{cat}E_0 D}{K_M}. \tag{A7}$$

If binding is rapid, the oligonucleotide, mRNA, and duplex forms will essentially be in equilibrium. The equilibrium relationship among O, M, and D, along with mass balances on O and M and the rate equation for X, provides four equations in the four unknowns O, M, D, and X. The solution for X is:

$$\frac{X}{M_T} = 1 - e^{-\frac{k_{cat}E_0}{K_M(1+K_D/O_T)}t}. \tag{A8}$$

Again, first-order kinetics are expected, in this case with a rate constant

$$k_{eff} = \frac{k_{cat}E_0}{K_M(1 + K_D/O_T)}. \tag{A9}$$

For all of the oligonucleotides on which RNase assays were performed, the equilibrium dissociation constant was significantly less than the oligonucleotide concentration. Therefore,

$$k_{eff} \approx \frac{k_{cat}E_0}{K_M}. \tag{A10}$$

Based on the specifications of the ribonuclease H supplier (Promega) and the published value of the Michaelis constant (0.2 μM, (Haruki et al., 2000)), the expected value of k_{eff} under conditions of high binding is ~0.1 s^{-1}, two orders of magnitude higher than observed (Fig. 7). Since we observed the predicted behavior for low k_a value and also observed the predicted plateau, the discrepancies in magnitude may be due to loss of activity of the RNase H enzyme through storage, exposure to buffer, or product inhibition.

The authors thank Arul Jayaraman for helpful discussions and review of the manuscript and assistance with the cloning and molecular biological techniques.

Support for this work was provided by the Whitaker Foundation and the Shriners Hospitals for Children. S.P.W. was partially supported by National Institutes of Health Biotechnology Training Grant GM08334.

REFERENCES

Andreyev, H. J., P. J. Ross, D. Cunningham, and P. A. Clarke. 2001. Antisense treatment directed against mutated Ki-ras in human colorectal adenocarcinoma. *Gut.* 48:230–237.

Bommarito, S., N. Peyret, and J. SantaLucia. 2000. Thermodynamic parameters for DNA sequences with dangling ends. *Nucleic Acids Res.* 28:1929–1934.

Cazenave, C., N. Loreau, N. T. Thuong, J. J. Toulme, and C. Helene. 1987. Enzymatic amplification of translation inhibition of rabbit beta-globin mRNA mediated by antimessenger oligodeoxynucleotides covalently linked to intercalating agents. *Nucleic Acids Res.* 15:4717–4736.

Ding, Y., and C. E. Lawrence. 2001. Statistical prediction of single-stranded regions in RNA secondary structure and application to predicting effective antisense target sites and beyond. *Nucleic Acids Res.* 29:1034–1046.

Eckardt, S., P. Romby, and G. Sczakiel. 1997. Implications of RNA structure on the annealing of a potent antisense RNA directed against the human immunodeficiency virus type 1. *Biochemistry.* 36:12711–12721.

Goodchild, J., E. D. Carroll, and J. R. Greenberg. 1988. Inhibition of rabbit beta-globin synthesis by complementary oligonucleotides: identification of mRNA sites sensitive to inhibition. *Arch. Biochem. Biophys.* 263: 401–409.

Haruki, M., Y. Tsunaka, M. Morikawa, S. Iwai, and S. Kanaya. 2000. Catalysis by *Escherichia coli* ribonuclease HI is facilitated by a phosphate group of the substrate. *Biochemistry.* 39:13939–13944.

Helene, C., and J. J. Toulme. 1990. Specific regulation of gene expression by antisense, sense and antigene nucleic acids. *Biochim. Biophys. Acta.* 1049:99–125.

Ho, S. P., Y. Bao, T. Lesher, R. Malhotra, L. Y. Ma, S. J. Fluharty, and R. R. Sakai. 1998. Mapping of RNA accessible sites for antisense experiments with oligonucleotide libraries. *Nat. Biotechnol.* 16:59–63.

Jaeger, J. A., D. H. Turner, and M. Zuker. 1989. Improved predictions of secondary structures for RNA. *Proc. Natl. Acad. Sci. U.S.A.* 86: 7706–7710.

Jayaraman, A., S. P. Walton, M. L. Yarmush, and C. M. Roth. 2001. Rational selection and quantitative evaluation of antisense oligonucleotides. *Biochim. Biophys. Acta.* 1520:105–114.

Juan, V., and C. Wilson. 1999. RNA secondary structure prediction based on free energy and phylogenetic analysis. *J. Mol. Biol.* 289:935–947.

Lima, W. F., V. Brown-Driver, M. Fox, R. Hanecak, and T. W. Bruice. 1997. Combinatorial screening and rational optimization for hybridization to folded hepatitis C virus RNA of oligonucleotides with biological antisense activity. *J. Biol. Chem.* 272:626–638.

Lima, W. F., B. P. Monia, D. J. Ecker, and S. M. Freier. 1992. Implication of RNA structure on antisense oligonucleotide hybridization kinetics. *Biochemistry.* 31:12055–12061.

Mathews, D. H., M. E. Burkard, S. M. Freier, J. R. Wyatt, and D. H. Turner. 1999a. Predicting oligonucleotide affinity to nucleic acid targets. *RNA.* 5:1458–1469.

Mathews, D. H., J. Sabina, M. Zuker, and D. H. Turner. 1999b. Expanded sequence dependence of thermodynamic parameters improves prediction of RNA secondary structure. *J. Mol. Biol.* 288:911–940.

Matveeva, O., B. Felden, S. Audlin, R. F. Gesteland, and J. F. Atkins. 1997. A rapid in vitro method for obtaining RNA accessibility patterns for complementary DNA probes: correlation with an intracellular pattern and known RNA structures. *Nucleic Acids Res.* 25:5010–5016.

Matveeva, O., B. Felden, A. Tsodikov, J. Johnston, B. P. Monia, J. F. Atkins, R. F. Gesteland, and S. M. Freier. 1998. Prediction of antisense oligonucleotide efficacy by in vitro methods. *Nat. Biotechnol.* 16: 1374–1375.

Milner, N., K. U. Mir, and E. M. Southern. 1997. Selecting effective antisense reagents on combinatorial oligonucleotide arrays. *Nat. Biotechnol.* 15:537–541.

Mir, K. U., and E. M. Southern. 1999. Determining the influence of structure on hybridization using oligonucleotide arrays. *Nat. Biotechnol.* 17:788–792.

Patzel, V., U. Steidl, R. Kronenwett, R. Haas, and G. Sczakiel. 1999. A theoretical approach to select effective antisense oligodeoxyribonucleotides at high statistical probability. *Nucleic Acids Res.* 27:4328–4334.

Patzel, V., J. zu Putlitz, S. Wieland, H. E. Blum, and G. Sczakiel. 1997. Theoretical and experimental selection parameters for HBV-directed antisense RNA are related to increased RNA-RNA annealing. *Biol. Chem.* 378:539–543.

Rivas, E., and S. R. Eddy. 1999. A dynamic programming algorithm for RNA structure prediction including pseudoknots. *J. Mol. Biol.* 285: 2053–2068.

Roth, C. M., and M. L. Yarmush. 1999. Nucleic acid biotechnology. *Annu. Rev. Biomed. Eng.* 1:265–297.

SantaLucia, J., H. T. Allawi, and P. A. Seneviratne. 1996. Improved nearest-neighbor parameters for predicting DNA duplex stability. *Biochemistry.* 35:3555–3562.

Scherr, M., J. J. Rossi, G. Sczakiel, and V. Patzel. 2000. RNA accessibility prediction: a theoretical approach is consistent with experimental studies in cell extracts. *Nucleic Acids Res.* 28:2455–2461.

Schwille, P., F. Oehlenschlager, and N. G. Walter. 1996. Quantitative hybridization kinetics of DNA probes to RNA in solution followed by diffusional fluorescence correlation analysis. *Biochemistry.* 35: 10182–10193.

Sczakiel, G., M. Homann, and K. Rittner. 1993. Computer-aided search for effective antisense RNA target sequences of the human immunodeficiency virus type 1. *Antisense Res. Dev.* 3:45–52.

Smith, L., K. B. Andersen, L. Hovgaard, and J. W. Jaroszewski. 2000. Rational selection of antisense oligonucleotide sequences. *Eur. J. Pharm. Sci.* 11:191–198.

Stein, C. A. 1999. Two problems in antisense biotechnology: in vitro delivery and the design of antisense experiments. *Biochim. Biophys. Acta.* 1489:45–52.

Sugimoto, N., S. Nakano, M. Katoh, A. Matsumura, H. Nakamuta, T. Ohmichi, M. Yoneyama, and M. Sasaki. 1995. Thermodynamic parameters to predict stability of RNA/DNA hybrid duplexes. *Biochemistry.* 34:11211–11216.

Tabaska, J. E., R. B. Cary, H. N. Gabow, and G. D. Stormo. 1998. An RNA folding method capable of identifying pseudoknots and base triples. *Bioinformatics.* 14:691–699.

Vickers, T. A., J. R. Wyatt, and S. M. Freier. 2000. Effects of RNA secondary structure on cellular antisense activity. *Nucleic Acids Res.* 28:1340–1347.

Walter, A. E., D. H. Turner, J. Kim, M. H. Lyttle, P. Muller, D. H. Mathews, and M. Zuker. 1994. Coaxial stacking of helixes enhances binding of oligoribonucleotides and improves predictions of RNA folding. *Proc. Natl. Acad. Sci. U.S.A.* 91:9218–9222.

Walton, S. P., C. M. Roth, and M. L. Yarmush. 2000. Antisense technology. *In* The Biomedical Engineering Handbook, 2nd Ed. CRC Press LLC, Boca Raton, FL. 103-1–103-19.

Walton, S. P., G. N. Stephanopoulos, M. L. Yarmush, and C. M. Roth. 1999. Prediction of antisense oligonucleotide binding affinity to a structured RNA target. *Biotechnol. Bioeng.* 65:1–9.

Wu, M., and I. Tinoco. 1998. RNA folding causes secondary structure rearrangement. *Proc. Natl. Acad. Sci. U.S.A.* 95:11555–11560.

Zuker, M. 1989. On finding all suboptimal foldings of an RNA molecule. *Science.* 244:48–52.

Zuker, M., and A. B. Jacobson. 1995. "Well-determined" regions in RNA secondary structure prediction: analysis of small subunit ribosomal RNA. *Nucleic Acids Res.* 23:2791–2798.

Zuker, M., J. A. Jaeger, and D. H. Turner. 1991. A comparison of optimal and suboptimal RNA secondary structures predicted by free energy minimization with structures determined by phylogenetic comparison. *Nucleic Acids Res.* 19:2707–2714.